HOSTED BY

Available online at www.sciencedirect.com

ScienceDirect

Journal of Computational Design and Engineering 3 (2016) 370–384

www.elsevier.com/locate/jcde

Material feature representation and identification with composite surfacelets

Wei Huang[a], Yan Wang[b,*], David W. Rosen[b]

[a]HP Labs, Palo Alto, CA 94304, United States
[b]School of Mechanical Engineering, Georgia Institute of Technology, Atlanta, GA 30332, United States

Received 14 November 2015; received in revised form 16 June 2016; accepted 26 June 2016
Available online 1 July 2016

Abstract

Computer-aided materials design requires new modeling approaches to characterize and represent fine-grained geometric structures and material compositions at multiple scales. Recently, a dual-Rep approach was developed to model materials microstructures based on a new basis function, called surfacelet. As a combination of implicit surface and wavelets, surfacelets can efficiently identify and represent planar, cylindrical, and ellipsoidal geometries in material microstructures and describe the distribution of compositions and properties. In this paper, these primitive surfacelets are extended and composite surfacelets are proposed to model more complex geometries. Composite surfacelets are constructed by Boolean operations on the primitives. The surfacelet transform is applied to match geometric features in three-dimensional images. The composition of the material near the identified features can then be modeled. A cubic surfacelet and a v-joint surfacelet are developed to demonstrate the reverse engineering process of retrieving material compositions from material images.

Keywords: Heterogeneous modeling; Implicit surface; Feature identification; Surfacelet transform

1. Introduction

The application of heterogeneous materials has become common in modern product design such as composites and porous media. Computational design tools for such materials, with higher complexity than traditional homogeneous ones, will be a critical component in the realization of modern products with complex functions systematically. It is foreseen that future computer-aided design systems will include the modules for materials design so that the design of functional materials and structures can be integrated for optimal product development.

In the integrated materials-product design, not only a multi-scale modeling method is needed to represent material microstructures in computer, it is also important to allow for integrated reverse engineering so that models reconstructed from material images can be modified and optimized, because imaging techniques have been the major methods to characterize microstructures and properties in materials design. Therefore, it is critical that the geometric features of interest as microstructures can be easily identified and extracted from the images. Those geometric features embody the key characteristics of physical properties in materials design. The modification and optimization of the parameters in those features are the major means to engineer materials to meet the design target. Additionally, the successful identification and representation of the features are important for the abstraction and simplification of the material composition distributions in modeling. Therefore, an integrated and efficient approach for feature identification, modeling, and analysis for materials and microstructures is the goal of this research.

A new dual-Rep modeling approach for materials design was recently proposed to represent property distributions in heterogeneous materials [1]. The core component of this representation is a new basis function, called surfacelet. A surfacelet is a combination of implicit surface and wavelet basis. The surfacelet-based modeling approach enables us to

*Corresponding author. Fax: +1 404 894 9342.
E-mail addresses: huang@hp.com (W. Huang), yan.wang@me.gatech.edu (Y. Wang), david.rosen@me.gatech.edu (D.W. Rosen).
Peer review under responsibility of society of Cad /Cam Engineers.

http://dx.doi.org/10.1016/j.jcde.2016.06.005

capture material distributions at multiple scales. The corresponding reverse engineering method to identify features and reconstruct surfacelet models directly from material images was also developed. This construction process is based on a so-called *surfacelet transform*. The surfacelet formulation will be introduced in Section 2.3 in details.

In our previous work [1–3], three primitive surfacelets (planar, cylindrical, and ellipsoidal) were proposed. It has been demonstrated that with the properly chosen surfacelets, geometric features in images can be identified. For instance, the cylindrical surfacelet can be used to recognize fibers in composite materials. The 3D ridgelet with the planar shape can find orientations of grain boundaries in polycrystalline structures. However, in more general heterogeneous materials, the geometric features in materials can be more complex than some primitive shapes. Identifying the locations and orientations of complex features by primitives becomes inefficient and imprecise. In this paper, the concept of composite surfacelets is proposed, where different combinations of existing surfacelets can be used to construct new surfacelets with more complex geometries. Compared to the primitive shapes in the original surfacelet formulation, composite surfacelets allow for modeling complex geometries with reduced surfacelet parameter dimensions, because the combined primitives are treated with rigid-body transformation during translation and rotation operations. Therefore, there is a need of more complex surfacelets than the primitives. Surfacelets with a better match of complex features can improve the efficiency and accuracy of feature recognition. The extension of the available surfacelets also increases the flexibility of the surfacelet model for different materials.

It is desirable that the surfacelet model can be applied to both design new materials and redesign existing ones. In reverse engineering, the identified geometric features provide the basic structural information of material composition as boundaries and interfaces. Yet, more detailed material composition information such as gradient and distribution should also be modeled in addition to the geometric features. The surfacelet model provides an abstraction of such information in the parametric form so that structure–property relationship can be established. With the parametric model, material property and performance can be optimized by choosing the best composition and distribution with the optimal shape parameters.

In this paper, the concept of composite surfacelet is demonstrated by two specific ones, cubic and v-joint surfacelets. The cubic surfacelet is constructed from six planar ridgelets, whereas the v-joint surfacelet is constructed from two cubic surfacelets. These two composite surfacelets are then used for the identification of complex microstructural features such as in composites with their implicit surface components. The distribution of materials in the interphase region of composites between two adjacent materials is modeled with the wavelet component from the feature identification results, which is also demonstrated. The novelty of the proposed approach is that the new concept of composite surfacelet allows for identifying and modeling of complex microstructures and heterogeneous material distributions with high-level abstraction from images by several parameters, which cannot be done with traditional image-based feature recognition approaches.

In the remainder of the paper, a literature review of the most relevant work is given in Section 2. The details of surfacelet formulation and surfacelet based material feature identification and modeling are also described. In Section 3, the construction and representation of the cubic v-joint surfacelet are described. The methods of applying the cubic and v-joint surfacelets in feature identification are presented in Sections 4 and 5 respectively. In Section 6, examples are given to illustrate how composite surfacelets can be used in modeling distributions of materials.

2. Background

2.1. Heterogeneous materials and multiscale modeling

Various modeling methods for solid heterogeneous materials have been proposed [4], such as volume meshes or voxels [5,6], property interpolation [7–9], local feature compositions [10–13], implicit surface blending [14,15], multiscale porous modeling [16–19], and multi-phase stochastic geometry based on voxels [20], surfaces [21], and Markov random field [22]. Those methods focused on representation of geometries or continuous distributions of volume composition, whereas the feature identification of materials was not considered.

2.2. Image-based feature recognition methods

Edges define the boundaries between regions in an image, which help with feature recognition. The edge detection methods [23,24] can be categorized into two groups: search-based and zero-crossing based. The search-based methods capture the feature edges by first computing edge strength and then searching for the local maxima in a direction to match the edge profile. The edge strength and searching direction can be measured and defined in different forms, such as the magnitude and the direction of the gradient of the image intensity. The gradient is usually represented by the first order derivative. On the other hand, the zero-crossing based methods search for zero crossings based on the second-order derivatives to detect feature edges.

Other methods of identifying geometric features from images have also been developed. For instance, the Radon transform [25] has been applied to identify lines in 2D images [26,27]. Similarly, the Hough transform was applied to recognize spherical features in 3D images [28].

For the purpose of materials design, not only the pixels on the feature edges need to be recognized, it is also important to represent geometric information, such as shapes, dimensions, locations and orientations, of the features at a higher-level abstraction than just pixels. Edge detection methods only extract feature boundaries as pixels. We also need to detect more complex features than simple linear and spherical shapes. The feature identification approach based on composite

surfacelets can improve the efficiency and accuracy of feature identification.

It is well known that the method of convolution is able to find the largest integrals and therefore identify geometric features. However, in this paper, it is not used for the following three reasons. Firstly, the method of convolution only returns the largest integrals for feature identification, and other smaller integrals are ignored for restoration. However, these smaller integrals are also important in the full reconstruction of the material images by inverse surfacelet transform. Secondly, although image is the main medium for us to visualize material compositions and structures, it does not provide means of *modeling* and *abstraction* that are essential for the design purpose. Therefore, we need high-level and parametric description of material features, instead of pixel-level representation. The method of convolution only gives pixel-wise description for feature identification, which is not enough for general design purpose. Lastly, the searching procedure of convolution is always pixel by pixel. In contrast, the step size in the proposed surface integrals is flexible and adjustable. This can enhance the searching efficiency in feature identification.

2.3. Surfacelet, surfacelet transform, surfacelet based material feature identification and modeling

Surfacelet is generally defined as [1]

$$\psi_{a,b,\mathbf{p}}(\mathbf{r}) = a^{-1/2}\psi(a^{-1}\rho_{b,\mathbf{p}}(\mathbf{r}))$$

where $\mathbf{r} = (x, y, z)$ is the location in a domain with x, y, and z coordinates in the Euclidean space, $\psi : \mathbb{R} \to \mathbb{R}$ is a wavelet function, $a \in \mathbb{R}^+$ is a non-negative *scaling factor*, $\rho_{b,\mathbf{p}} : \mathbb{R}^3 \to \mathbb{R}$ is a function so that $\rho_{b,\mathbf{p}}(x, y, z) = 0$ implicitly defines a surface (e.g. plane, cylinder, ellipsoid), with the *translation factor* $b \in \mathbb{R}^+$ and vector $\mathbf{p} \in \mathbb{R}^m$ determining the location and shape of surface. The implicit surface component ρ represents a specific shape and can be constructed by defining a set of shape parameters $\mathbf{p}$. The wavelet component ψ provides a multi-resolution modeling method with the convenience of local control. With the defined parameters for shape control, transformation, and scaling, surfacelets enable multi-scale modeling for heterogeneous materials. The wavelet component of a surfacelet represents a field or a distribution, whereas the zero or other iso-value levels of the surface component describes the directional surface singularity or discontinuity of the distribution along the surface boundary. The combination of the two components models a local material distribution with surface boundaries. Therefore, it is able to represent geometric boundaries and internal material distributions simultaneously in a unified form.

As a primitive surfacelet, a 3D ridgelet that represents plane singularities is defined as

$$\psi_{a,b,\alpha,\beta}(\mathbf{r}) = a^{-1/2}\psi(a^{-1}(\cos\beta\cos\alpha\cdot x + \cos\beta\sin\alpha\cdot y + \sin\beta\cdot z - b))$$

where b, $\alpha \in [0, 2\pi)$, and $\beta \in [-\pi/2, \pi/2]$ are location parameters corresponding to rotations around z- and y-axes in the Euclidean space. Similarly, a cylindrical surfacelet can be defined as

$$\psi_{a,b,\alpha,\beta,r_1,r_2}(\mathbf{r}) = a^{-1/2}\psi(a^{-1}[r_1(\cos\beta\cos\alpha\cdot x + \cos\beta\sin\alpha\cdot y + \sin\beta\cdot z - b)^2 + r_2(-\sin\alpha\cdot x + \cos\alpha\cdot y)^2])$$

where b, α, and β are location parameters, and r_1 and r_2 are shape parameters that determine the size and shape of the cylinder. An ellipsoidal surfacelet is defined as

$$\psi_{a,b,\alpha,\beta,r_1,r_2,r_3}(\mathbf{r}) = a^{-1/2}\psi(a^{-1}[r_1(\cos\beta\cos\alpha\cdot x + \cos\beta\sin\alpha\cdot y + \sin\beta\cdot z - b)^2 + r_2(-\sin\alpha\cdot x + \cos\alpha\cdot y)^2 + r_3(-\sin\beta\cos\alpha\cdot x + \sin\beta\sin\alpha\cdot y + \cos\beta\cdot z)^2])$$

Surfacelet bases can be used to interpolate and approximate material properties in modeling materials distributions. In addition, the surfacelet transform has been developed to reconstruct surfacelet models from images as a reverse engineering process. The surfacelet transform of three-dimensional (3D) material images is illustrated in Fig. 1, First, a surface defined in the surfacelet, for instance, an elliptic cylinder, is placed in the 3D Euclidean space of the 3D images with specific translation distance b from the origin, rotational angle α about z-axis, and rotational angle β about y-axis. A surface integral operation is applied to the 3D images. During the process, the pixels that are located on the cylindrical surface are identified and the corresponding pixel values are added together as the surface integral value. This surface integral is then stored as a point value in the surfacelet space, which uses α, β, and b as coordinates or indices. By varying the locations and orientations of the surface systematically with discrete step sizes, a series of surface integral values can be obtained and stored in a 3D matrix with α, β, and b indices. In other words, the surface integrals are calculated by varying the values of location parameters. Then 1D wavelet transforms along the b axis direction in the surfacelet space are performed for all α's and β's. The results are surfacelet coefficients for all rotational angles. In general, the dimension of the matrix in the transformed surfacelet space corresponds to the number of location parameters used in the surfacelet. In a similar vein, the dimension of the transformed surfacelet space can be extended by varying both location and shape parameters. Then the size and shape of the cylinder surface are not fixed.

In the actual implementation of the surfacelet transform, the surfacelets with discretized locations and orientations are arranged to cover the entire image domain. Then the summation of pixel values that are on each surface is calculated. If the

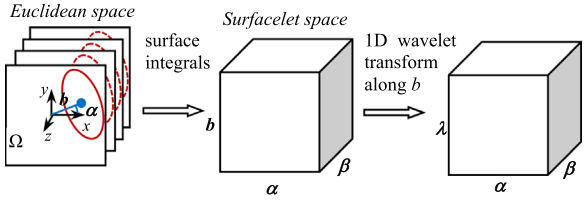

Fig. 1. The surfacelet transform process.

distance between a pixel and the surface is smaller than a threshold, the pixel is regarded as on the surface. The summations as the approximated surface integrals are further converted to surfacelet coefficients by the wavelet transform.

When surfacelets are used in feature identification, shape parameters including surface types and dimensions are determined based on the target features. Surfaces of the target features are represented with certain shape parameters. The parameter values are chosen to match the shape and size of the physical object that needs to be identified. With the application of surfacelet transform to 3D images of materials, the positions and orientations of the material features can be identified. Because the largest surface integral values are associated with those surfacelets that overlap with the features, the locations and orientations of those features can then be identified by searching the largest surface integral values. The identified features also provide prior knowledge as constraints to reconstruct the original images from surfacelet coefficients by the *inverse surfacelet transform* [3]. Obviously the shape parameters can also vary during feature identification process. However, with the increased dimensionality of surfacelet transformed space, the computational cost also increases. In this study, the values of shape parameters are kept fixed.

As the result of the surfacelet transform, the coefficients in the surfacelet space are used to capture material features and distributions in the original image space. The largest surfacelet integral values or coefficients indicate the best fits of the features by those surfacelets with some particular shape and location parameters, assuming that the features of interest have higher pixel values than the rest of the image. If this is not the case, the image can always be inverted. The largest pixel value of a grayscale image is typically 255. For a pixel with the value p in the original image, the corresponding one in the inverted image is $255-p$. Therefore, the location and orientation information of the most prominent features can be identified from the largest surfacelet integrals.

When surfacelets are used in representing microstructures, the material distributions in Euclidean space can be modeled with the combinations of surfacelet bases. After the locations and orientations of major features in 3D images are identified by surfacelet transform, the material distributions or fields are then approximated with the major features by choosing proper wavelets and combination coefficients [1,2].

Notice that the major research issue for feature identification with surfacelet is how to construct representative patterns with the implicit surface in order to make the surfacelet transform effective in recognizing the feature. For modeling material distributions, the selection of wavelet functions becomes important. Any admissible wavelets can be used in the surfacelet formulation, such as commonly used Haar, Daubechies, Morlet, etc. The choice relies on the efficiency of modeling specific distribution types.

3. Composite surfacelets

In order to increase the flexibility and efficiency of feature identification, the existing primitive surfacelets are extended to composite surfacelets. Designing a composite surfacelet is to apply Boolean operations to primitives so that complex surfaces can be represented implicitly.

The cubic and v-joint surfacelets proposed here can identify features with straight-line boundaries, often seen in material microstructures. For instance, nanoscale cubes are observed in UMF-20 alloy [29], $BiPO_4$ nanorods [30], and 2,6-diamino-3,5-dinitropyrazine-1-oxide (LLM-105) microtubes [31]. They can be represented by the cubic surfacelet. The fracture surface of powder particles in powder composites is naturally planar since powder materials are brittle, such as ceramic-metal composite Al_2O_3–Fe used in energy and automobile industries [32]. Other examples are the microstructures of silver based conductor QM14 [33], $BaTiO_3$ ceramics [34], MgO-PSZ [35] and GDC electrolyte on the anode tube in solid-oxide fuel cells [36]. Although the grains in these materials have linear edges, they have varied numbers of sides in the polyhedral shapes. The cubic surfacelet becomes insufficient. Those microstructures can be more efficiently represented by the v-joint surfacelet.

3.1. Cubic surfacelet

With selected parameters, the composite surfacelet with a cubic shape is able to identify the features with cubic or rectangular boundaries. Geometrically the cubic surfacelet is constructed by three sets of parallel ridgelets or planar surfacelets that are perpendicular to x-, y-, and z-axes respectively. As shown in Fig. 2, the first set of two planes, denoted by $x_\perp$, is represented implicitly as $\rho_1(x,y,z) = (x-c)(x-d) = 0$. Similarly, the $y_\perp$ and $z_\perp$ sets are represented as $\rho_2(x,y,z) = (y-a)(y-b) = 0$ and $\rho_3(x,y,z) = (z-e)(z-g) = 0$ respectively. Here, a, b, c, d, e, and g are translation parameters of the individual ridgelets.

Six parameters are used to decide the location and orientation of a cubic surfacelet in 3D space, three for the translation along x-, y-, and z-axes and three for the rotation about these axes. Suppose the size of the box is $l_1 \times l_2 \times l_3$ for the cubic surfacelet. They are constant once the shape of the cubic surfacelet is determined. The translation parameters a, b, c, d, e and g are

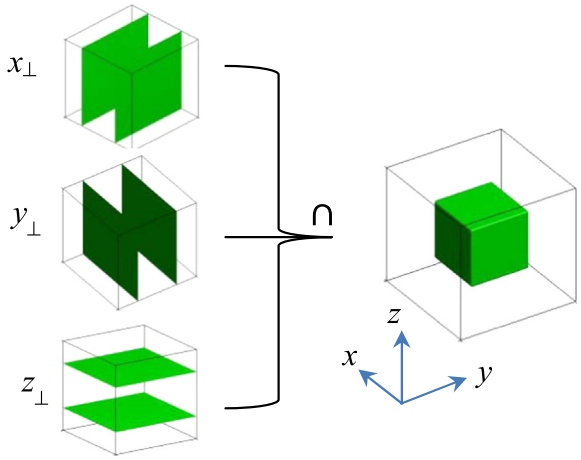

Fig. 2. The construction of cubic surfacelet from three sets of two parallel ridgelets perpendicular to x-, y-, and z-axes.

related by $b=a+l_1$, $d=c+l_2$, and $g=e+l_3$. Therefore, the three translation parameters along the x-, y-, and z-axes can be assigned as the translation of the center point of the cube. With the translation and rotation involved, the implicit representation of the three sets of planes ρ_1, ρ_2, and ρ_3 can be derived.

According to the R-function representation [37,38], the union of two volumes or half-spaces defined implicitly by functions ρ_1 and ρ_2 is $\min(\rho_1,\rho_2)$ and can also be represented as

$$\rho_{1\cup 2}=\frac{1}{2}\left(\rho_1+\rho_2-\sqrt{\rho_1^2+\rho_2^2-2\rho_1\rho_2}\right)=0 \tag{1}$$

Here, function ρ is defined such that its value is negative inside a domain enclosed by the boundary $\rho(x,y,z)=0$ and positive outside. The intersection of two volumes is $\max(\rho_1,\rho_2)$ and can also be represented as

$$\rho_{1\cap 2}=\frac{1}{2}\left(\rho_1+\rho_2+\sqrt{\rho_1^2+\rho_2^2-2\rho_1\rho_2}\right)=0 \tag{2}$$

Notice that Eqs. (1) and (2) are chosen among different possible versions of R-function representations such that the union or intersection of a function to itself (i.e. $\rho_1=\rho_2$) is precisely equivalent to the original min and max functions. This property is necessary when the functions are used to represent the complete distributions instead of just zero-level boundaries of the domains. In our case, the complete distributions of materials need to be captured. In addition, R-function has better continuity than the min and max functions. Similarly, the cube formed by ρ_1, ρ_2, and ρ_3 is

$$\rho_c=\frac{1}{2}\left(\rho_{1\cap 2}+\rho_3+\sqrt{\rho_{1\cap 2}^2+\rho_3^2-2\rho_{1\cap 2}\rho_3}\right)=0 \tag{3}$$

The final form of ρ_c' in the cubic surfacelet is

$$\rho_c'(l_1,l_2,l_3;m,n,k,\alpha,\beta,\gamma;x,y,z)=\frac{1}{2}\left(\rho_{1\cap 2}'+\rho_3'+\sqrt{\rho_{1\cap 2}'^2+\rho_3'^2-2\rho_{1\cap 2}'\,\rho_3'}\right)=0$$

where ρ' is the surface after the translation and rotation operations are applied to ρ, parameters m, n, and k correspond to the translations along x-, y-, and z-axis respectively, and α, β, and γ are the rotational angles about the three axes. Instead of using min and max functions, which may provide computational convenience for Boolean operations, R-functions are applied here to maintain the algebraic form of surfacelets.

3.2. V-joint surfacelet

General polyhedral shapes other than the rectangular ones are also seen in microstructures. The rectangular feature is only a special case of the polyhedral ones. The grain shapes of many traditional materials are very close to polyhedrons, such as all forms of polygonal crystals in many alloys. One example is Al_2O_3 particle shown in Fig. 3(a). The two-phase structure of Al_2O_3–Fe obtained through infiltration of the porous ceramic matrix formed by the Al_2O_3 powder in Fig. 3(a) is shown in Fig. 3(b).

Another significant characteristic about the powder composite materials is that the grains are compactly packed and the binding phase is in a network formed with nodes and connecting edges, as shown in Fig. 3(b). Together with the fact that the polyhedral grain features have more irregular shapes than the rectangular feature, it is not effective that we still use the scheme in Section 3.1 to represent or identify the grains. Instead, representing and identifying the binding phase including nodes and edges, such as the Fe phase in Fig. 3, is a better choice.

The v-joint surfacelet is a composite surfacelet that unites two narrow and rectangular cubic surfacelets to form a V shape. The V shape can identify both the node locations and edge orientations simultaneously. The construction of the v-joint surfacelet is described as follows and illustrated in Fig. 4. The shape parameters of the v-joint surfacelet are the width W, the edge length L, and the depth D. Two narrow cubic surfacelets with the same sizes are combined at the ends along the edge length direction to form a *pivot* with a *v-joint angle* θ, by the union operation for implicit surfaces. During the surfacelet transform, the shape parameters are fixed. They are adjusted to match those of the connection phase of the material at the beginning of the surfacelet transform. The

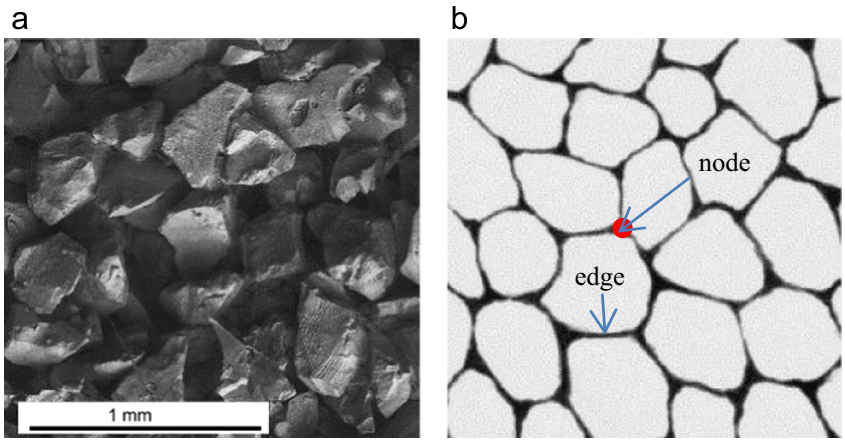

Fig. 3. Microstructure of Al_2O_3 and Al_2O_3–Fe composites [25]: (a) SEM image of Al_2O_3 ceramic particles, (b) image of ceramic–metal composites (dark region is Fe, and light region is Al_2O_3).

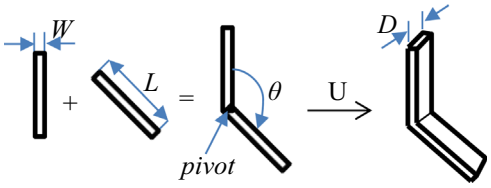

Fig. 4. The construction of v-joint composite surfacelet based on two cubic surfacelets.

location parameters, including the overall translation distances, rotation angles, and v-joint angle θ, vary. Note that θ is not defined as a shape parameter. This allows for more flexibility in pattern matching.

The union between the two rectangular implicit surfaces in the v-joint surfacelet is done by the R-function similar to Eq. (1). There are also seven location parameters to locate a v-joint surfacelet, three (m, n, and k) for translation, three (α, β, and γ) for orientation, and the v-joint angle θ. The three translation parameters along the x-, y-, and z-axis can be assigned as the translation of the pivot. The rotation angles around the x-, y-, and z-axis are α, β and γ respectively. The rotation and translation methods for the v-joint surfacelet are exactly the same as the cubic surfacelet. The final form of the implicit surface in the v-joint surfacelet is

$$\rho'_v(W,L,D;m,n,k,\alpha,\beta,\gamma,\theta;x,y,z)=\frac{1}{2}\left[\rho'_{c1}\left(W,L,D;m,n,k+\frac{L}{2},\alpha,\beta,\gamma;x,y,z\right)+\rho'_{c2}\left(W,L,D;m,n,k+\frac{L}{2},\alpha,\beta,\gamma+\theta;x,y,z\right)\right]-\frac{1}{2}\sqrt{\begin{array}{l}\rho'^2_{c1}(W,L,D;m,n,k+\frac{L}{2},\alpha,\beta,\gamma;x,y,z)+\rho'^2_{c2}(W,L,D;m,n,k+\frac{L}{2},\alpha,\beta,\gamma+\theta;x,y,z)\\ -2\rho'_{c1}(W,L,D;m,n,k+\frac{L}{2},\alpha,\beta,\gamma;x,y,z)\cdot\rho'_{c2}(W,L,D;m,n,k+\frac{L}{2},\alpha,\beta,\gamma+\theta;x,y,z)\end{array}}=0$$

where ρ'_{c1} and ρ'_{c2} are the two cubic surfaces in the v-joint surfacelet after transformation is applied. An example for identifying the connection features with v-joint composite surfacelets will be given in Section 5.

4. Feature identification with cubic surfacelets

The feature identification with composite surfacelets is based on the largest surface integrals, similar to the one based on the primitive surfacelets [2,27]. Typically, the locations and orientations of the features are of interest. Geometric information of the target features, such as the shape and size, are prior knowledge and assumed to be known. The features are captured by examining the surface integrals. If necessary, some image processing methods can be applied to increase the contrast and highlight the features as a pre-processing step.

4.1. Feature identification

When a surfacelet is overlapped with the feature (e.g., a cylindrical surfacelet is overlapped with a fiber surface), its corresponding surface integral value is larger than those of other surfacelets. Therefore surface integrals help determine the positions and orientations of the target feature geometries. If there is only one feature geometry to identify, its position and orientation can be directly estimated by the corresponding surfacelet with the largest integral. This can be realized by sorting the surface integrals from the results of surfacelet transform. If there are more than one feature geometry, the largest integral for one feature geometry can be very close to the one for another feature geometry, because some surfacelets can be overlapped with multiple feature geometries. In this case, the integrals are grouped into different clusters according to their positions and orientations. The largest integral or the best estimate based on some criteria in each cluster determines the feature geometry. This clustering process is regarded as an averaging or homogenization scheme in the multi-resolution surfacelet representation.

In existing materials, it is common that the cubic or rectangular particles of interest have various sizes. In order to identify all feature geometries, the shape parameters of the cubic surfacelet are chosen to be identical to the smallest particle. For those particles that are larger than the surfacelet, multiple surfacelets with the largest integrals are needed to identify the location and orientation of one particle. The union of these surfacelets, which is the overall profile of the surfacelets, will be able to show the location and orientation of a particle. For those particles that almost have the same size as the surfacelet, only the largest integral is needed to identify the location and orientation of one particle.

4.2. Demonstration

In this section, the cubic surfacelet is used to identify the microstructures of nano-C60 [39], as shown in Fig. 5(a). In this example, a small representative portion of the image with one particle is used to illustrate, as shown in Fig. 5(b). The same image is stacked three times to form the 3D slices in this example. The images are treated as 3D cross-section slices of the particle. The top and bottom boundaries of the particle are not included in the three images, as shown in Fig. 5(c). Therefore, the size of the particle along z-axis direction is assumed to be large, and the corresponding shape parameter l_3 is set to be a large value. The size of each image is 76×76, thus the total number of pixels for three images is $P=76\times 76\times 3=17{,}328$.

The shape parameters of the cubic surfacelet are $l_1=1.34$, $l_2=1$, and $l_3=3$, which are designed to match the size of the particle. The translation along the z-axis is set as zero. The number of cubic surfacelets used is $m\times n\times\alpha\times\beta\times\gamma=10\times 10\times 1\times 1\times 6=600$. The surfacelet with the largest integral is used for identification. The feature identification result is shown in Fig. 6. Note that the numbers of discrete parameter values for translation and

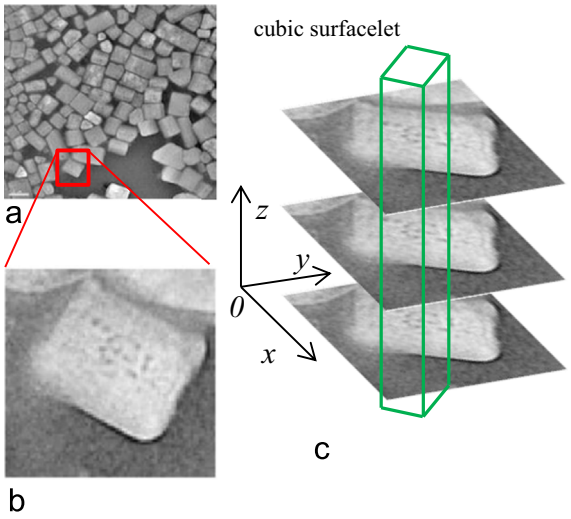

Fig. 5. 3D images of nano-C60 particle: (a) Nano-C60 particles [39], (b) the image portion used in the example cubic surfacelet, and (c) three identical images stacked in parallel.

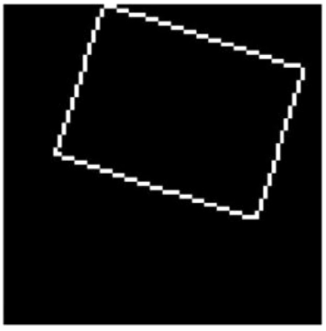

Fig. 6. Identifying a rectangular feature with a cubic surfacelet with matching shape parameters.

rotation (m, n, α, β, γ) are determined by choosing the desirable resolution. Larger numbers are needed if finer resolution is chosen and more accurate feature positions and orientations need to be identified. Obviously more surfacelets require higher computational cost. Users need to make tradeoffs so that all important features are identified with affordable computational time. Nevertheless, the ranges of these values should always be chosen such that the entire 3D image space is covered by the translated and rotated surfacelets.

As stated in Section 4.1, particles in images may have varied sizes. In order to identify all feature geometries, the dimensions of the cubic surfacelet are chosen to be identical to the smallest particle. Therefore, to demonstrate the generality of feature identification based on the cubic surfacelet, we intentionally choose a cubic surfacelet that is smaller than the rectangular particle. The number of surfacelets used is $m \times n \times \alpha \times \beta \times \gamma = 20 \times 20 \times 1 \times 1 \times 30 = 12000$. The shape parameters of the cubic surfacelet are $l_1 = l_2 = 0.5$, and $l_3 = 3$. They are designed to match the size of the smallest particle. The translation along the z-axis is set as zero. Because $l_1 = l_2$ thus the chosen cubic surfacelet is self-symmetric, the range of rotation angles α, β, γ can be reduced to $[0, \pi/2]$. The feature identification result is shown in Fig. 7. It can be seen that the size, location, and orientation of the particle can be

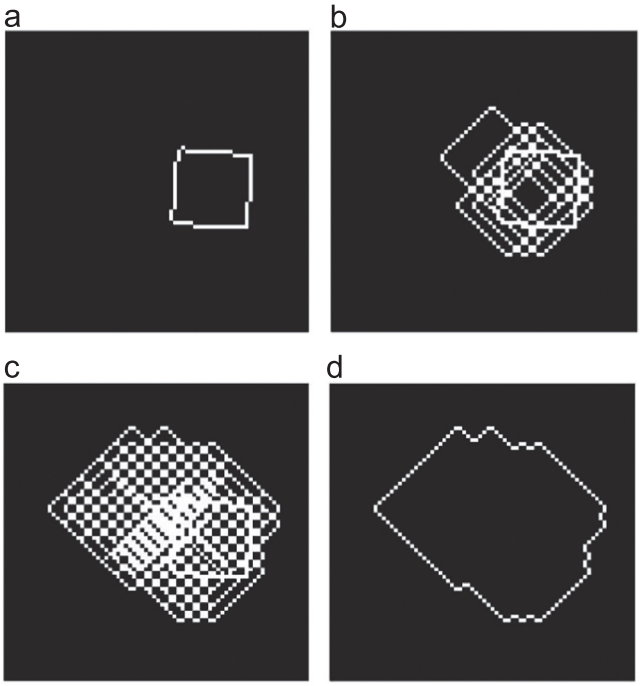

Fig. 7. Identifying rectangular features with cubic surfacelets in smaller size: (a) the largest one integral, (b) the largest 50 integrals, (c) the largest 456 integrals, and (d) the overall profile by union.

better recognized if more integrals with the largest values are utilized. Implemented in Matlab and tested on a personal computer with a 2.5 GHz central processing unit (CPU) and 8 GB random access memory, the identification process takes about 5 s of CPU time.

The identified feature can be applied for the reconstruction of the original images by inverse surfacelet transform [3]. The reconstruction is conducted with a constrained conjugate-gradient method. Only the boundary pixels are added as constraints. In this example, there is no need to translate the cubic surfacelet in the z-direction, i.e. $k = 0$. To decrease the computational cost, the size of each image is reduced to 20×20, thus the total number of pixels for three images is $P = 20 \times 20 \times 3 = 1200$. The number of surfacelets used in reconstruction is $m \times n \times \alpha \times \beta \times \gamma = 8 \times 8 \times 1 \times 1 \times 10 = 640$. The results of reconstructed images are shown in Fig. 8, where one to twenty integrals with the largest values are chosen to be constraints respectively. The data compression rate is 47%. Note that the traditional convolution and Hough transform are not designed for image compression and reconstruction.

5. Feature identification with V-joint surfacelets

In this section, the feature identification approach based on v-joint surfacelets is described. The advantage of applying the v-joint shape is that the vertex of a joint can be explicitly identified.

5.1. Feature identification

From the example in Fig. 3(b), it is seen that the gray scale pixel values and the widths of the nodes and edges for the

metal binding phase are not uniform. The image can be processed so that the binding phase has larger pixel values. After the surfacelet transform is applied, most of the largest integrals will be from the bright and wide nodes and edges. Therefore, in order to identify those darker or narrower feature geometries, more surfacelets are needed.

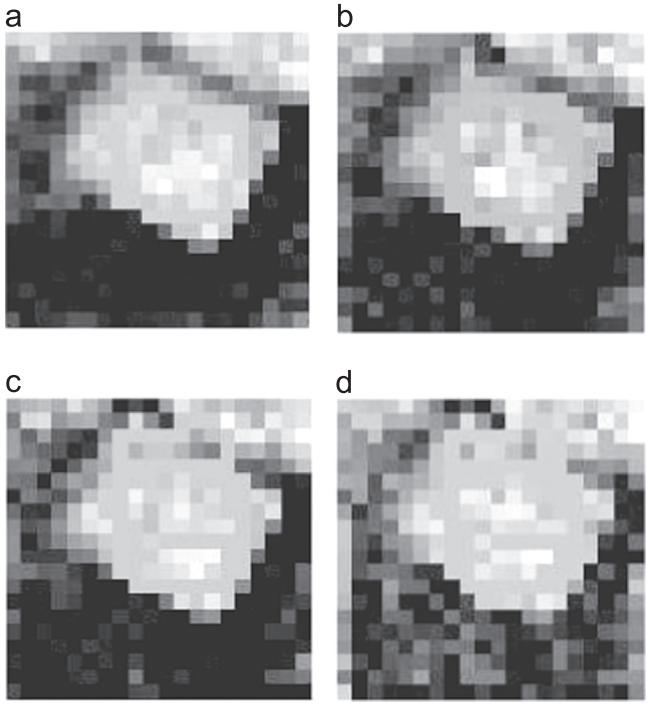

Fig. 8. Image reconstruction results with different constraints of cubic surfacelets: (a) the largest one integral, (b) the largest five integrals, (c) the largest ten integrals, and (d) the largest twenty integrals.

Most of the surfacelets for those bright and wide nodes and edges do not exactly overlap with the feature geometries. Therefore, in order to clearly capture the feature geometries, those surfacelets with correct locations and orientations should be extracted through a clustering process. In this paper, we use a simple scheme of identifying locations and orientations of v-joint surfacelets by their averages within each cluster for each feature. The process of feature identification is graphically illustrated in Fig. 9 and summarized as the flow chart in Fig. 10.

The seven steps are described as follows.

In the first step, the shape parameters of the v-joint surfacelet are designed to match the edge lengths and angles in-between. Then the surfacelet transform is applied to obtain the surface integrals, as illustrated in Fig. 9(a).

In the second step, the number of surfacelets with the largest integrals is chosen such that all important feature geometries can be covered, as illustrated in Fig. 9(b).

In the third step, these surfacelets are grouped into clusters based on relative locations and orientations so that all surfacelets in the same cluster are for the same feature geometry, as illustrated in Fig. 9(c).

In the fourth step, the average pivot location and orientation of each cluster are calculated. A new surfacelet with the average location and orientation is created, and all old surfacelets are discarded as the process of dimensionality reduction, as illustrated in Fig. 9(d). After this step, the

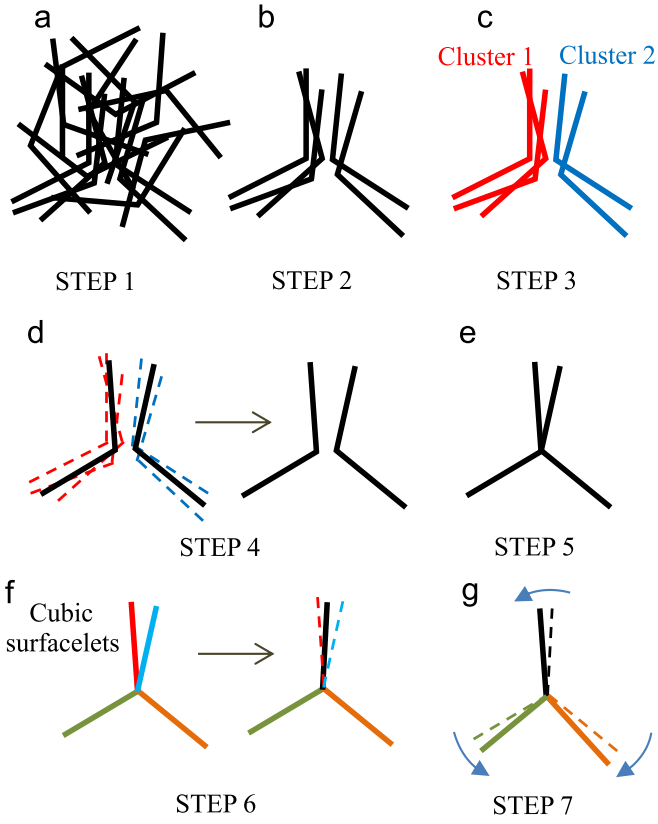

Fig. 9. The illustration of the feature identification process with the v-joint surfacelet.

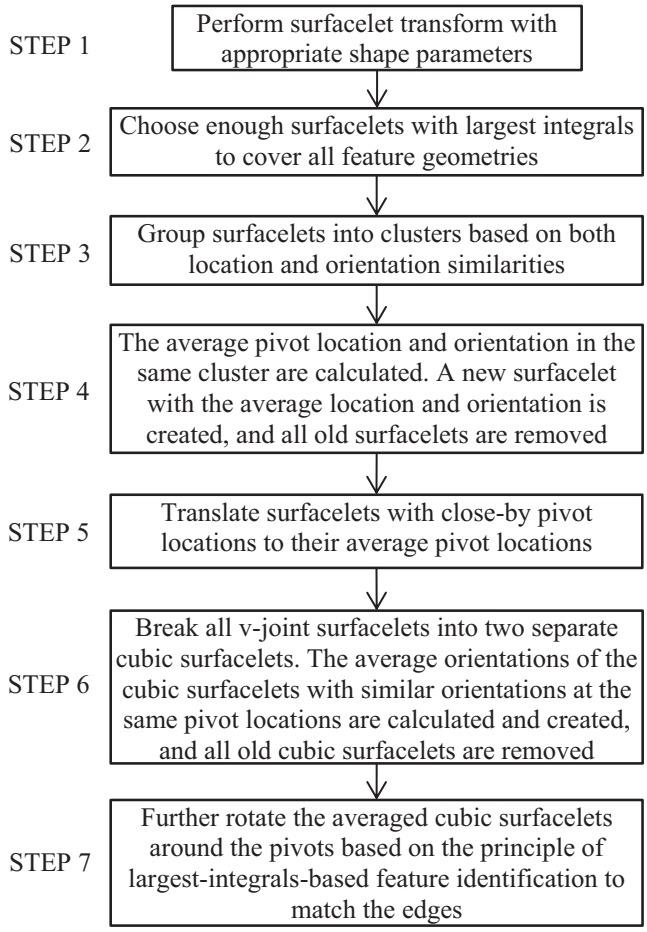

Fig. 10. The process of the feature identification with the v-joint surfacelet.

resolution in the surfacelet domain is reduced, and the number of surfacelets for feature identification is significantly reduced. It should be noted that if there are multiple surfacelets for one feature geometry, the pivots of these surfacelets are distributed around the node. Because the nodes in the images actually correspond to multiple pixels, the average location is able to approximately reflect the geometric center of the node.

For feature identification, the center of the node is desired. Since at least two v-joint surfacelets are needed to cover three edges at one node, these two surfacelets should be properly coordinated to form a one-node three-branch geometry. Therefore, in the fifth step, those surfacelets with close-by pivot locations are translated to their average pivot location so that two surfacelets for one node are connected and the locations of the nodes are identified, as illustrated in Fig. 9(e). The surfacelets with different orientations to cover the three edges of one node should not be clustered together by average. The reason is as follows. If one of the three edges has a very large width, then most surfacelets in the cluster may be located on that edge. Then the average pivot is likely to be pulled towards that edge instead of reflecting the geometric center, because the surfacelets on that edge account for a larger weight. Therefore, the clusters are formed based on different orientations of v-joints within some threshold. With the separate clustering and averaging for the multi-branch cases, there will be no more than two surfacelets at one node so that one edge cannot overweight another. After finding the average pivot locations, the v-joint surfacelets with similar orientations at the same pivot location should be rotated to the average orientation.

To improve the accuracy of identification, a v-joint surfacelet can be further broken into two separate cubic surfacelets and rotate each cubic surfacelet separately so that the angles can be further fine-tuned. Therefore, in the sixth step, the average orientations of the cubic surfacelets that share the same pivot location and have the similar orientations are calculated. The old cubic surfacelets can also be removed for better clarity and accuracy, as illustrated in Fig. 9(f). In order to make the surfacelets better match the edges, the averaged cubic surfacelets are further rotated around the pivots based on the principle of largest integrals, as illustrated in Fig. 9(g).

5.2. Demonstration

The Al_2O_3–Fe composite in Fig. 3 is used to demonstrate the v-joint feature identification. Three slices of images are also used in this example. To better demonstrate the details, only a portion of the images is used here. The spatial domain in the images is normalized to be $[-1, 1]$ for all ranges of x, y, and z directions. The ranges of the translation parameters are m, n, and $k \in [-1, 1]$, and the ranges of the rotation angles are

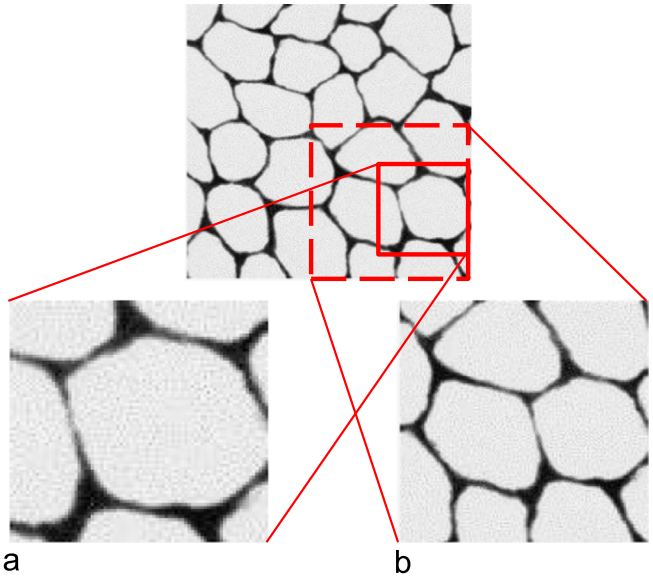

Fig. 11. Two portions of Al_2O_3–Fe composite images to test the v-joint surfacelet: (a) image with one grain, (b) image with multiple grains.

α, β, and $\gamma \in [0, 2\pi]$ to ensure that the surfacelets cover all target features.

Two portions are selected from the original image to test the scalability. The first one contains one grain as shown in Fig. 11 (a), and the second one has multiple grains as shown in Fig. 11 (b). Because the largest-integrals-based feature identification method requires that the feature to be identified should have a larger gray scale value than the rest of the image, the images are inverted first.

A 2-D case is first tested where only one image is considered. Based on the estimated average size of the metal phase in the image, the shape parameters of the v-joint surfacelet are chosen as $W=0.02$, $L=0.4$, and $D=4$. W is estimated to approximate the width of the boundary region, L is about half of the length of a boundary edge (because two surfacelet branches approximate one boundary edge), and D is the approximated depth of a boundary edge. The v-joint angle $\theta=100^\circ$ is fixed. This can significantly reduce the computational time of surfacelet transform, because the dimension of the reciprocal surfacelet space is reduced without varying the v-joint angle. The number of surfacelets used here is $m \times n \times \alpha \times \beta \times \gamma = 30 \times 30 \times 1 \times 1 \times 30 = 27000$. There is no need to translate the v-joint surfacelet in the z-axis direction, i.e. $k=0$.

With the largest-integrals-based feature identification method, the identification results for different numbers of largest integrals are compared in Fig. 12. It can be seen that since the values of pixels within the metal phase are not equal to each other, neither the widths of the nodes and edges, many surfacelets are needed to identify those features with either bright pixels or narrow geometries. As shown in Fig. 12, when more than 100 largest integrals are used, most feature geometries in the image are covered after STEP 1. Then the surfacelets with similar locations and orientations are clustered and averaged. The result after STEP 4 is shown in Fig. 13(a). The number of surfacelets is reduced from 150 to 12. The result after STEP 6 is shown in Fig. 13(b). The number of surfacelets is further reduced from 12 to 9. The result after STEP 7 is shown in Fig. 13(c). Fig. 13(d) shows the cubic

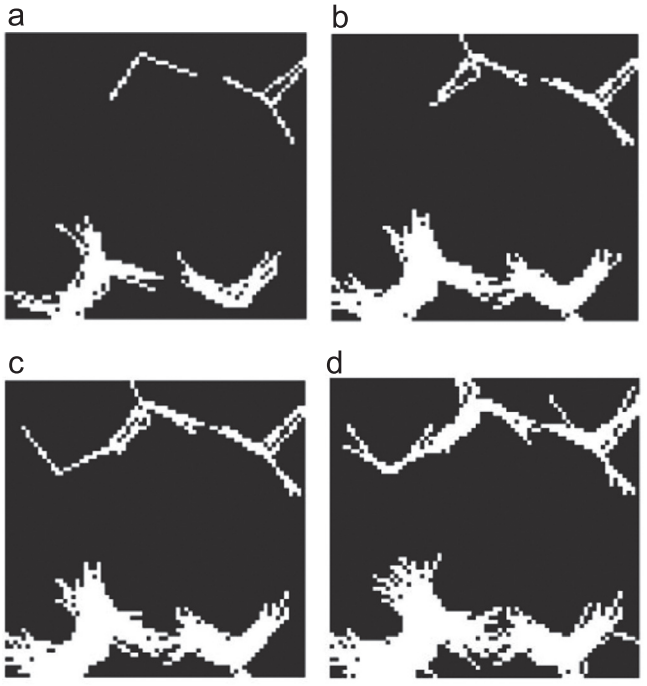

Fig. 12. Features identified after STEP 1, with different numbers of largest integrals: (a) largest 30 integrals, (b) largest 80 integrals, (c) largest 100 integrals, and (d) largest 150 integrals.

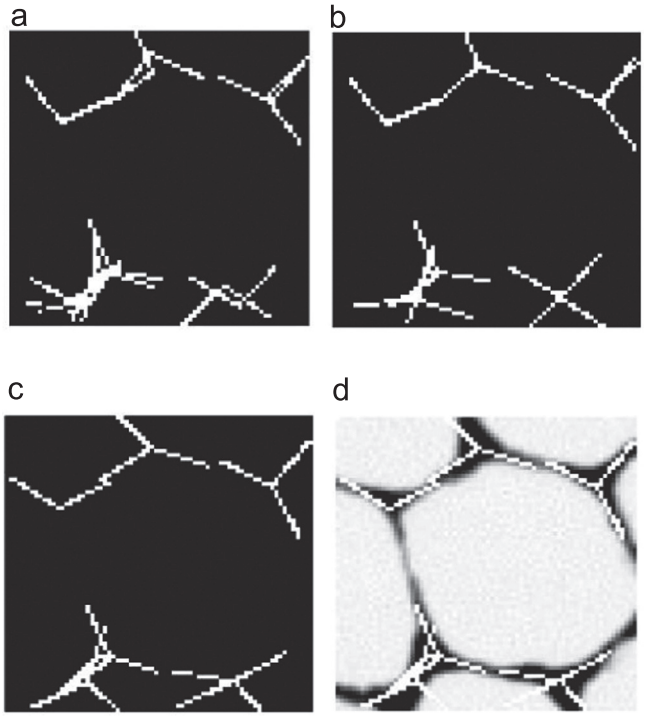

Fig. 13. The intermediate results during the process of the feature identification: (a) result of STEP 4 (12 surfacelets), (b) result of STEP 6 (9 surfacelets), (c) result of STEP 7, and (d) result matching the original image.

surfacelets derived from the v-joint surfacelets match the feature in the original image fairly well.

In order to test the scalability of the proposed method, the image with multiple grains is also used. The identification result is shown in Fig. 14. Notice that in this example the width of the v-joint is small because it needs to match the thinnest feature in the original image. It will be increased if the original feature width is larger. In contrast, traditional Radon or Hough transform only considers edge feature without thickness information.

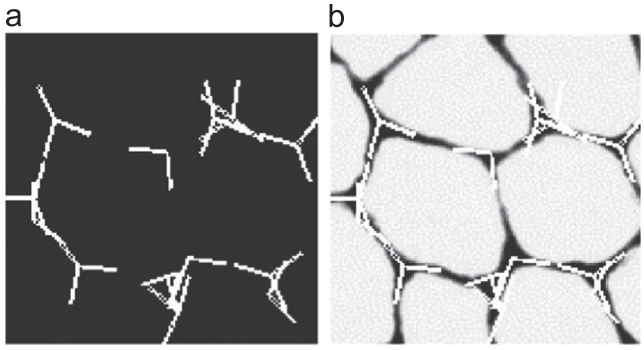

Fig. 14. The identification result for the image with multiple grains: (a) the feature identification result, (b) result matching the original image.

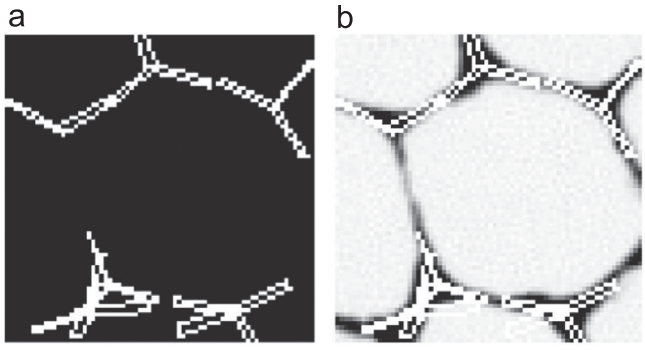

Fig. 15. The identification result with thickness recognition for the image with one grain: (a) the feature identification result, (b) result matching the original image.

In the above examples, the feature identification is only for the positions and orientations of boundaries. The thickness information was captured. This can be realized by treating the thickness as the extra dimension in the surfacelet space. Therefore, a modified feature identification process is also proposed by tweaking the seventh step. Instead of only rotating the averaged cubic surfacelets around the pivots, the thickness is also adjusted based on the principle of largest-integrals-based feature identification to match the boundaries. In the same example, the thickness is adjusted in the range of [0.01, 0.03] with step size of 0.005. The results for one-grain and multiple-grain images are shown in Figs. 15 and 16 respectively. The identification process for these 2D examples takes about 10 s of CPU time. The major target of identification in this example includes the corners or vertices of the cellular structure. Once they are identified, the structure can be reconstructed with some post-processing procedures based on the edge information provided by the partially covered v-joints.

It can be seen from Figs. 15 and 16 that not only the positions and orientations of boundaries, but also the variable thickness can be identified. The extra shape parameter helps better identify features with less post-processing of clustering. However, the increased dimension in the surfacelet space requires more computation. In other words, a trade-off is needed to find a good combination of surfacelet transform and post-processing for both performance and computational cost.

The v-joint identification is also tested in 3D cases. Fig. 17 shows the three slices of images used to test the v-joint surfacelet, and Fig. 18 shows the result of identification. The number of surfacelets used here is $m \times n \times \alpha \times \beta \times \gamma = 20 \times 60 \times 10 \times 1 \times 20 = 240000$, which includes more rotations than the above 2D examples ($10 \times 1 \times 20$ vs. $1 \times 1 \times 30$). In both cases, $\beta = 1$ because the accuracy of results was reasonable even without rotation about y-axis, which was to reduce computational cost. The difference between 2D/2.5D and 3D applications is just the dimensionality of surfacelet parameter space. 3D cases have higher dimensions and require more

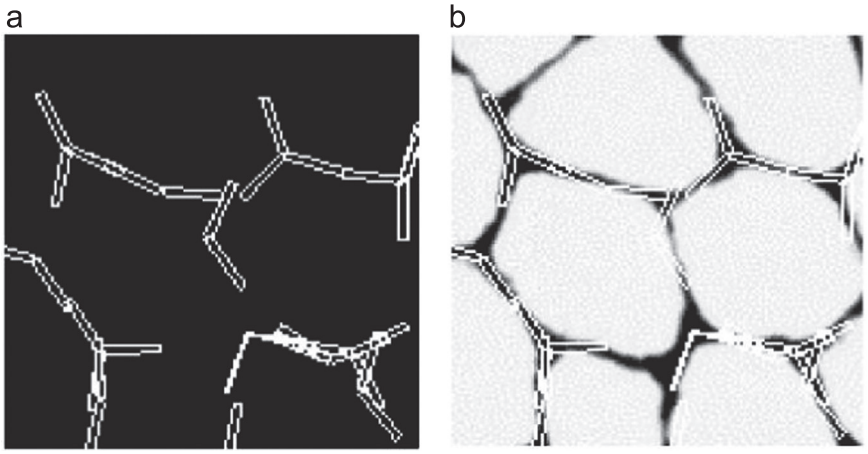

Fig. 16. The identification result with thickness recognition for the image with multiple grains: (a) the feature identification result, (b) result matching the original image.

Fig. 17. Slices of images used to test the v-joint surfacelet.

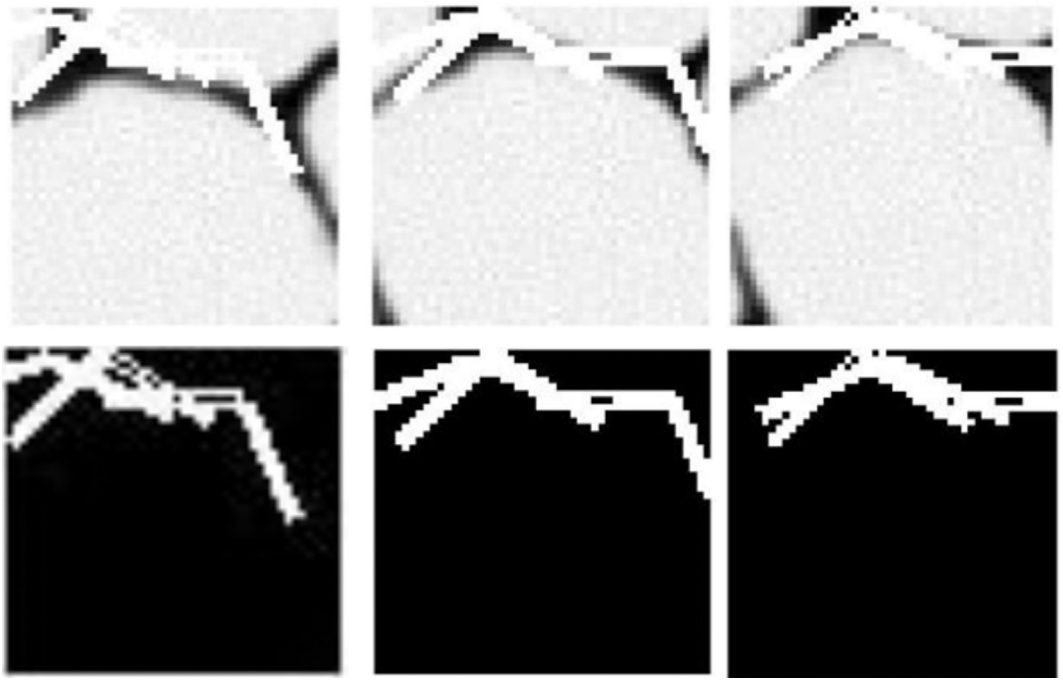

Fig. 18. The identification result of 3D images.

computational time. The computational time in the 3D example of Fig. 18 is about 800 CPU seconds.

6. Material distribution modeling

Once material boundaries are identified using the procedures described in previous sections, heterogeneous material distributions with phase boundaries can be modeled with wavelet components. In this section, two examples are used to illustrate material distribution modeling by combing identified boundaries with wavelets.

The first example is to illustrate that the wavelet component in surfacelet allows us to naturally represent distributions in a multi-resolution fashion. In a two-phase material system, material composition is typically modeled with composition ratio, also known as order parameter. As shown in Fig. 19, the value of order parameter changes from 0 to 1 across phase boundary. The distribution can be approximated by wavelets. Wavelet transform can be applied to the composition data, either from experiments or other models, and different combinations of wavelet bases can be chosen for the approximations at different resolutions. Here, Haar wavelet basis is used. As more wavelets of smaller scales with fine details are included, the wavelet model gradually converges to the original distribution. With the wavelets combined with the phase boundaries identified in Fig. 7, the distribution of composition with different levels of details can be modeled, as shown in Fig. 20.

The second example is to illustrate that physical properties can be modeled in a similar way. Fig. 21(a) shows the storage modulus map of the carbon fiber reinforced polymer composite measured by Gu et al. [40]. The fiber surface boundaries can be identified by cubic surfacelet, as shown in Fig. 21(b). 1D Mexican hat wavelet model of the modulus distribution shown in Fig. 21(c) is reconstructed from the measured data along the cross-section line in Fig. 21(a). By combining the wavelet model with the identified boundary, the modulus map modeled with surfacelet is shown in Fig. 21(d).

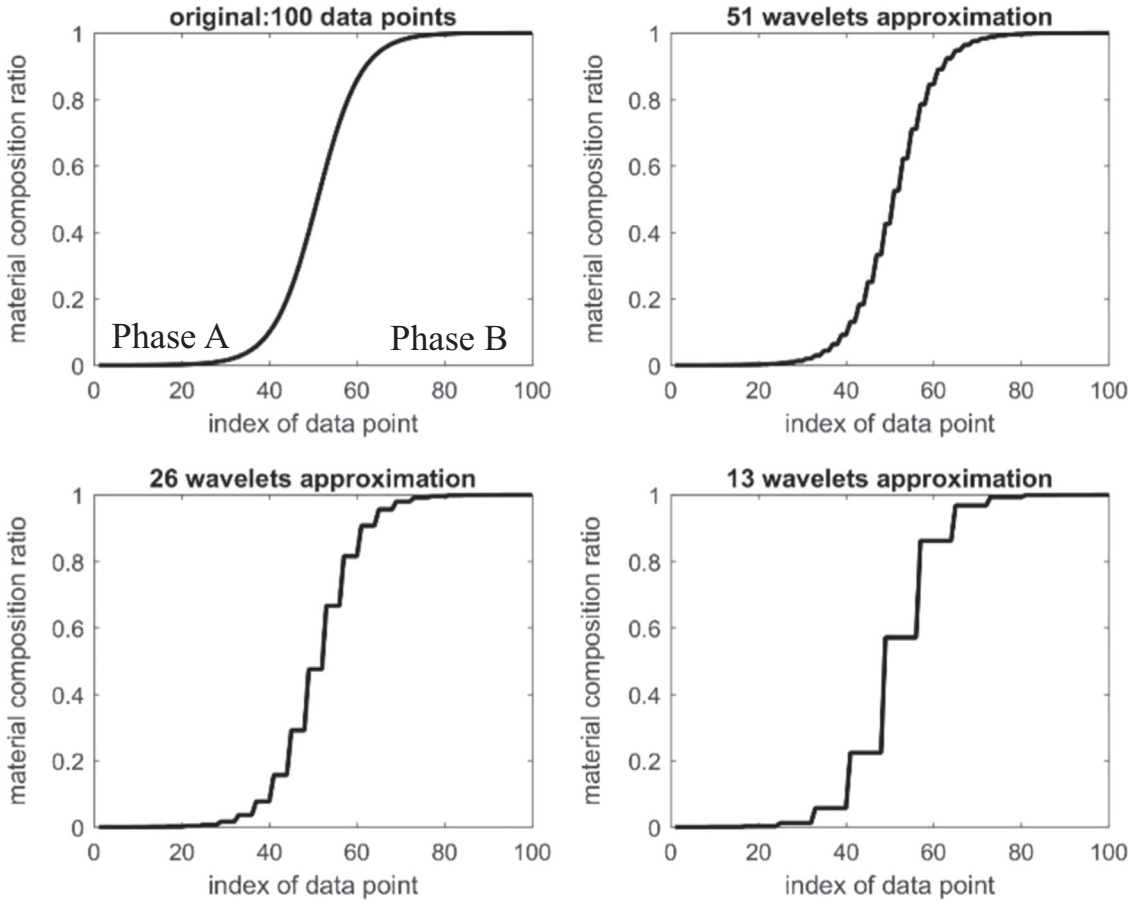

Fig. 19. Wavelets model phase distributions with multiple resolutions.

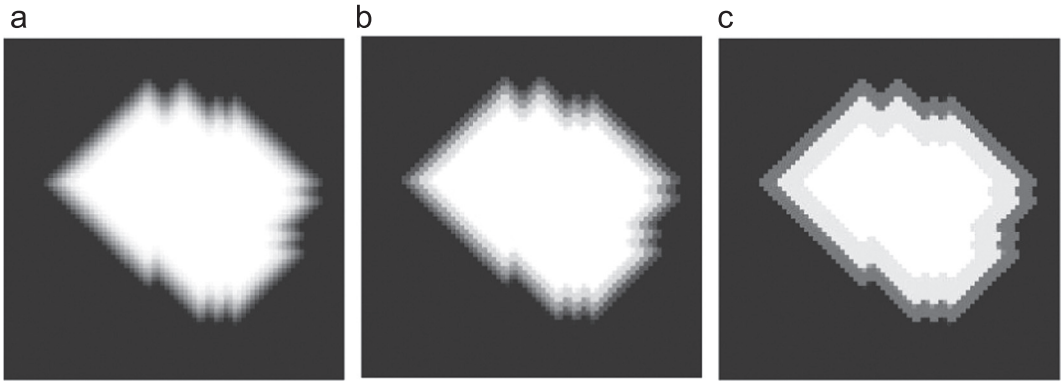

Fig. 20. Composite surfacelet models of phase distributions based on wavelets in Fig. 19 with different levels of details: (a) approximated distribution with 51 wavelets, (b) approximated distribution with 26 wavelets, and (c) approximated distribution with 13 wavelets.

7. Conclusion and future work

In this paper, a new concept of composite surfacelets is proposed to represent and identify complex microstructures. Composite surfacelets can be constructed from existing primitive or composite surfacelets. As two examples, cubic and v-joint surfacelets are developed to identify edge features. They are tested with microstructure images. The results show that with the surfacelet transform and the largest-integrals-based feature identification method, composite surfacelets are able to identify the locations, orientations and thickness of features. It should be noted that the concept of composite surfacelets is general. Composite surfacelets are not limited to these two demonstrated in this paper. More types of composite surfacelets can be designed and tailored for different microstructural features.

The identification approach presented in this paper is mainly for important features. If other details about material microstructures in images are of interest and the reconstruction of

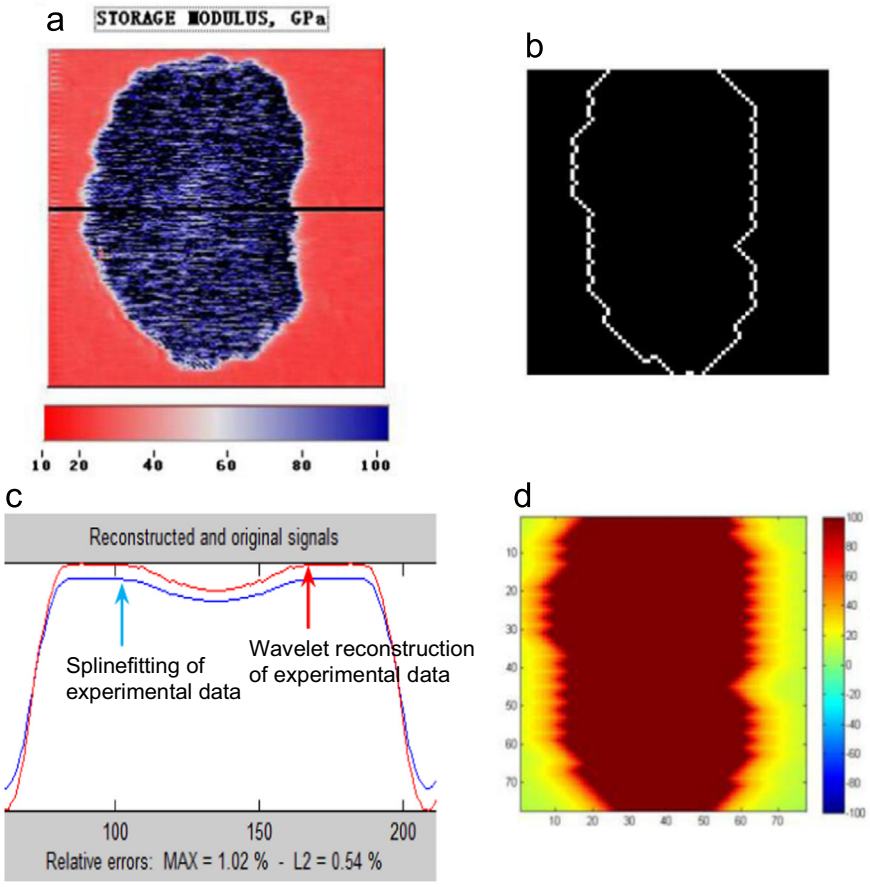

Fig. 21. Composite surfacelet modeling of property distribution in carbon fiber reinforced epoxy resin composite: (a) storage modulus map of fiber composite [41], (b) phase boundary identified with cubic surfacelet, (c) 1D wavelet model of modulus distribution measured along the line in (a), and (d) Surfacelet model of modulus map by combing wavelet model in (c) with the boundary in (b).

the original images is desired, the inverse surfacelet transform can be applied. More surfacelets are required if more details need to be captured and reconstructed.

Compared to traditional edge and feature detection methods, our proposed method extracts the important geometric features (shapes, sizes, locations, and orientations), which provide parametric-level information to determine material properties. That is, the proposed method uses only a few parameters to represent important features instead of pixels. The description of geometric features is based on the distribution or field, instead of explicit boundaries. The distribution is modeled with a higher-level abstraction than the pixel-level representation. The modeling of distribution by parameters is readily available for analysis of material properties and design optimization. Furthermore, compared to explicit representation methods for straight line or plane, there are two major benefits of using composite surfacelets. First, composite surfacelets allow us to represent features implicitly such as edge features with finite length by cubic or v-joint surfacelets. Second, cubic and v-joint surfacelets have non-zero thickness, which is very important in feature identification for the following reasons. With the simple union operation, cubic and v-joint surfacelets can be combined into a single implicit surface so that the geometry of a complex boundary can be represented by a group of simple implicit surfaces, as shown in the examples in this paper. In contrast, it is difficult to implement the union operation based on explicit boundary representation of straight lines or planes. Furthermore, edge boundaries, such as the Fe phase in the example of Al_2O_3–Fe composite in Section 5, usually have non-zero thickness. Therefore, v-joint surfacelets with non-zero thickness can capture the thickness information of such boundaries more accurately. In addition, it is possible to modify the sharp corner of v-joint surfacelet with smoother connection between two edges to match the actual shape of phase boundary more precisely, if the purpose is to identify the boundaries instead of vertices or corners. This can be done by applying the union of additional shape primitives in the composite surfacelet definition.

In this paper, only small portions of images in Figs. 5 and 11 are used to demonstrate the feature identification process. Reducing computational cost for the purpose of illustration was the major consideration. If the complete images are used, the number of surfacelets needs to be increased substantially so that the resolution in the surfacelet space is sufficiently high to identify all particles in the images. In other words, very small step sizes for translations and rotations are needed in order to identify those many particles. The challenge is when a surfacelet easily overlaps with multiple close-by particles. The surface integral value itself may not be enough to differentiate a good match with one particle from overlapping

with multiple particles. More information should be incorporated in feature identification [2]. Future work needs to consider the possible improvement of computational scheme for efficiency as well as the identification capability, for instance, to improve searching efficiency by sorting surface integral values with better data structures and restricting local search regions.

Conflict of interest

The authors do not have conflict of interest to declare.

Acknowledgments

This research was supported in part by the National Science Foundation under the Grant no. CMMI-1030385.

References

[1] Wang Y, Rosen DW. Multiscale heterogeneous modeling with surfacelets. *Comput-Aided Des Appl* 2010;**7**(5)759–76.
[2] Huang W. *Surfacelet based heterogeneous materials modeling*. School of Mechanical Engineering, Georgia Institute of Technology; 2014.
[3] Huang W, Wang Y, Rosen DW. Inverse surfacelet transform for image reconstruction with constrained-conjugate gradient methods. *J Comput Inf Sci Eng* 2014;**14**(2)021005.
[4] Kou XY, Tan ST. Heterogeneous object modeling: a review. *Comput-Aided Des* 2007;**39**(4)284–301.
[5] Bhashyam S, Shin KH, Dutta D. An integrated CAD system for design of heterogeneous objects. *Rapid Prototyp J* 2000;**6**(2)119–35.
[6] Koenig O, Fadel G. Application of genetic algorithms in the design of multi-material structures manufactured in rapid prototyping. In: Proceedings of the 10th annual solid freeform fabrication symposium; August 1999.
[7] Kumar V, Burns D, Dutta D, Hoffmann C. A framework for object modeling. *Comput-Aided Des* 1999;**31**(9)541–56.
[8] Qian X, Dutta D. Physics-based modeling for heterogeneous objects. *J Mech Des* 2003;**125**(3)416–27.
[9] Liu H, Maekawa T, Patrikalakis NM, Sachs EM, Cho W. Methods for feature-based design of heterogeneous solids. *Comput-Aided Des* 2004;**36**(12)1141–59.
[10] Siu YK, Tan ST. 'Source-based' heterogeneous solid modeling. *Comput-Aided Des* 2002;**34**(1)41–55.
[11] Qian X, Dutta D. Feature-based design for heterogeneous objects. *Comput-Aided Des* 2004;**36**(12)1263–78.
[12] Samanta K, Koc B. Feature-based design and material blending for free-form heterogeneous object modeling. *Comput-Aided Des* 2005;**37**(3)287–305.
[13] Martin T, Cohen E, Kirby RM. Volumetric parameterization and trivariate B-spline fitting using harmonic functions. *Comput Aided Geom Des* 2009;**26**(6)648–64.
[14] Park SM, Crawford RH, Beaman JJ. Functionally gradient material representation by volumetric multi-texturing for solid freeform fabrication. In: Proceedings of the 11th annual solid freeform fabrication symposium; August 2011.
[15] Biswas A, Shapiro V, Tsukanov I. Heterogeneous material modeling with distance fields. *Comput Aided Geom Des* 2004;**21**(3)215–42.
[16] Wang Y. Periodic surface modeling for computer aided nano design. *Comput-Aided Des* 2007;**39**(3)179–89.
[17] Fryazinov O, Vilbrandt T, Pasko A. Multi-scale space-variant FRep cellular structures. *Comput-Aided Des* 2013;**45**(1)26–34.
[18] Yoo DJ. Heterogeneous porous scaffold design for tissue engineering using triply periodic minimal surfaces. *Int J Precis Eng Manuf* 2012;**13**(4)527–37.
[19] Pasko A, Fryazinov O, Vilbrandt T, Fayolle PA, Adzhiev V. Procedural function-based modelling of volumetric microstructures. *Graph Model* 2011;**73**(5)165–81.
[20] Mishnaevsky LL. Automatic voxel-based generation of 3D microstructural FE models and its application to the damage analysis of composites. *Mater Sci Eng A* 2005;**407**(1)11–23.
[21] Huang W, Didari S, Wang Y, Harris TA. Generalized periodic surface model and its application in designing fibrous porous media. *Eng Comput* 2015;**32**(1)7–36.
[22] Liu X, Shapiro V. Random heterogeneous materials via texture synthesis. *Comput Mater Sci* 2015;**99**:177–89.
[23] Ziou D, Tabbone S. Edge detection techniques: an overview. *Int J Pattern Recognit Image Anal* 1998;**8**(4)537–59.
[24] Park JM, Murphey YL. *Edge detection in grayscale, color, and range images*. Wiley Encyclopedia of Computer Science and Engineering; 2008.
[25] Radon J. On the determination of functions from their integral values along certain manifolds. *IEEE Trans Med Imaging* 1986;**5**(4)170–6.
[26] Leavers VF, Boyce JF. The Radon transform and its application to shape parameterization in machine vision. *Image Vision Comput* 1987;**5**(2)161–6.
[27] Rosen DW, Jeong N, Wang Y. A method for reverse engineering of material microstructure for heterogeneous CAD. *Comput-Aided Des* 2013;**45**(7)1068–78.
[28] Niezgoda SR, Kalidindi SR, Hu X, Cingara GA, Wilkinson DS, Jain M, Wu P, Mishra RK, Arafin M, Szpunar J. Applications of the phase-coded generalized hough transform to feature detection, analysis, and segmentation of digital microstructures. *Comput Mater Contin* 2010;**14**(2)79–98.
[29] MacSleyne J, Uchic MD, Simmons JP, De Graef M. Three-dimensional analysis of secondary γ′ precipitates in René-88 DT and UMF-20 superalloys. *Acta Mater* 2009;**57**(20)6251–67.
[30] Xue F, Li H, Zhu Y, Xiong S, Zhang X, Wang T, Liang X, Qian Y. Solvothermal synthesis and photoluminescence properties of $BiPO_4$ nanococoons and nanorods with different phases. *J Solid State Chem* 2009;**182**(6)1396–400.
[31] Chen J, Qiao Z, Wang L, Nie F, Yang G, Huang H. Fabrication of rectangular 2,6-diamino-3,5-dinitropyrazine-1-oxide microtubes. *Mater Lett* 2011;**65**(6)1018–21.
[32] Konopka K, Olszówka-Myalska A, Szafran M. Ceramic–metal composites with an interpenetrating network. *Mater Chem Phys* 2003;**81**(2)329–32.
[33] Belavic D, Hrovat M, Pavlin M, Holc J. Some results obtained with diffusion patterning technology. *Microelectron Int* 2001;**18**(1)7–18.
[34] Brzozowski E, Castro MS, Foschini CR, Stojanovic B. Secondary phases in Nb-doped $BaTiO_3$ ceramics. *Ceram Int* 2002;**28**(7)773–7.
[35] Hao L, Lawrence J. CO_2 laser induced microstructure features in magnesia partially stabilised zirconia bioceramic and effects thereof on the wettability characteristics. *Mater Sci Eng A* 2004;**364**(1)171–81.
[36] Suzuki T, Funahashi Y, Yamaguchi T, Fujishiro Y, Awano M. Development of microtubular SOFCs. *J Fuel Cell Sci Technol* 2008;**5**:3.
[37] Rvachev VL. Theory of R-functions and some applications. (Naukova Dumka, 1982). [in Russian].
[38] Shapiro V. Real functions for representation of rigid solids. *Comput Aided Geom Des* 1994;**11**(2)153–75.
[39] TEM image of nano-C60 particle, available at ⟨http://www.britannica.com/EBchecked/media/137390/transmission-electron-microscopy-can-be-used-to-detect-and-characterize⟩.
[40] Gu Y, Li M, Wang J, Zhang Z. Characterization of the interphase in carbon fiber/polymer composites using a nanoscale dynamic mechanical imaging technique. *Carbon* 2010;**48**(11)3229–35.